

www.acsami.org Research Article

Design of Chemical Surface Treatment for Laser-Textured Metal Alloys to Achieve Extreme Wetting Behavior

Avik Samanta, Wuji Huang, Hassan Chaudhry, Qinghua Wang, Scott K. Shaw, and Hongtao Ding*



Cite This: ACS Appl. Mater. Interfaces 2020, 12, 18032-18045



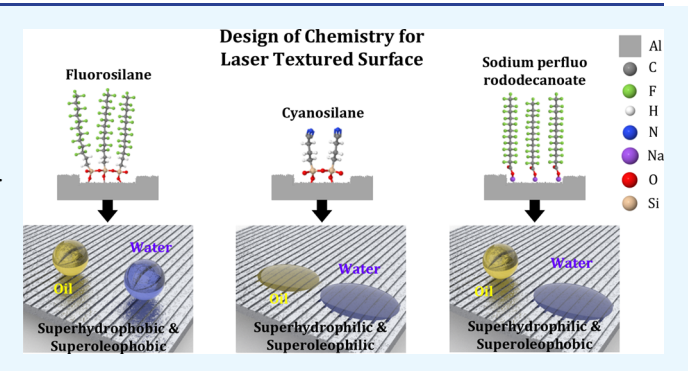
ACCESS

Metrics & More

Article Recommendations

Supporting Information

ABSTRACT: Extreme wetting activities of laser-textured metal alloys have received significant interest due to their superior performance in a wide range of commercial applications and fundamental research studies. Fundamentally, extreme wettability of structured metal alloys depends on both the surface structure and surface chemistry. However, compared with the generation of physical topology on the surface, the role of surface chemistry is less explored for the laser texturing processes of metal alloys to tune the wettability. This work introduces a systematic design approach to modify the surface chemistry of laser textured metal alloys to achieve various extreme wettabilities, including superhydrophobicity/superoleophobicity, superhydrophilicity/supero-



leophilicity, and coexistence of superoleophobicity and superhydrophilicity. Microscale trenches are first created on the aluminum alloy 6061 surfaces by nanosecond pulse laser surface texturing. Subsequently, the textured surface is immersion-treated in several chemical solutions to attach target functional groups on the surface to achieve the final extreme wettability. Anchoring fluorinated groups $(-CF_2-$ and $-CF_3)$ with very low dispersive and nondispersive surface energy leads to superoleophobicity and superhydrophobicity, resulting in repelling both water and diiodomethane. Attachment of the polar nitrile $(-C\equiv N)$ group with very high nondispersive and high dispersive surface energy achieves superhydrophilicity and superoleophilicity by drawing water and diiodomethane molecules in the laser-textured capillaries. At last, anchoring fluorinated groups $(-CF_2-$ and $-CF_3)$ and polar sodium carboxylate (-COONa) together leads to very low dispersive and very high nondispersive surface energy components. It results in the coexistence of superoleophobicity and superhydrophilicity, where the treated surface attracts water but repels diiodomethane.

KEYWORDS: design, laser texturing, chemical modification, superhydrophobicity, superoleophobicity, superhydrophilicity

■ INTRODUCTION

Employing pulsed laser-based surface processing methods to accomplish extreme wettability conditions on engineering materials has received significant attention over the past few decades. Processing with a pulsed laser is a maskless and contactless material removal method that possesses some unique advantages over other engineering methods, including flexibility, ease of automation, and a wide range of processing materials.1 The wettability of the laser-textured solid surface can be classified into two main categories, i.e., lyophobicity corresponding to apathy for a liquid and lyophilicity corresponding to affinity for a liquid.^{2,3} In general, wettability of a surface is quantified by contact angle (θ) , which is the angle at the solid-liquid interface between gas and solid through liquid. Lyophobicity and lyophilicity are mostly defined by $180^{\circ} > \theta > 90^{\circ}$ and $0^{\circ} \le \theta < 90^{\circ}$, respectively. To express extreme wettabilities, the word "super" is used as prefix in front of lyophobicity and lyophilicity. For example, superlyophobicity corresponds to $150^{\circ} < \theta < 180^{\circ}$, which has extreme apathy for a liquid. Similarly, superlyophilicity

corresponds to $0^{\circ} \leq \theta < 10^{\circ}$, which has an extreme affinity for a liquid. For the lyophobic surface, the roll-off angle $(\theta_{\text{roll-off}})$ is also used along with θ . It is a critical inclination angle at which the liquid droplet trends to slide/roll off the surface. Extreme wetting interactions at the solid—liquid interface play a crucial role in mobilizing global markets in many industrial processes and applications. Superlyophilic surfaces enhance the performance for catalysts, fuel cells and batteries, heat pipe wicks, dental implants, etc. Similarly, superlyophobic surfaces are increasingly used for antibacterial and antibiofouling, the drag reduction, and anticorrosion, and anticorrosion, applications.

Received: November 26, 2019 Accepted: March 25, 2020 Published: March 25, 2020





Surfaces with the coexistence of lyophobicity and lyophilicity have applications in oil—water separation.²⁰

The wetting behavior of textured solids varies based on three major factors at a solid-liquid interface: 21 (a) solid surface topography, (b) solid surface chemistry, and (c) liquid properties. Extensive knowledge has been obtained on physical topology generation by laser surface processing 1,22,23 for extreme wetting surfaces. Two main physical topologies have been extensively fabricated by pulsed laser processing where the laser pulse width ranges from femtosecond to nanosecond: (1) laser-induced periodic surface structures (LIPSSs), which possess laser-induced periodic surface ripples, 24-26 and (2) laser-inscribed hierarchical or dual-scale micro/nanosurface structures. 24,27,28 LIPSSs are produced by repetitive irradiation of the same area by multiple laser pulses at fluence levels in the regime of surface melting and resolidification. Key geometrical aspects of LIPSSs, such as periodicity and orientation, were effectively modulated by changing the laser texturing parameters including laser fluence, scanning velocity, number of pulses per irradiation point, angle of incidence, wavelength, and polarization and target material physical properties such as optical density, thermal conductivity, specific heat, laser absorptivity, and emissivity.²⁹ Laser-textured hierarchical surface structures or dual-scale structures consist of one structure at the higher scale (micron scale) and another structure at the lower scale (nanoscale) on top of higher scale structures. Hierarchical surface structures are often fabricated on the target substrate using short or ultrashort laser pulses. 30-36 The higher scale structures include microcolumns, 30 microspikes, 32 microtrench, 31,33 micromatrix, 34 and spot array. 35,36 On the other hand, nanoscale structures on top of higher scale features include LIPSSs³² or random nanostructures.³⁵ Few works have also been reported to use a continuous wave (CW) fiber laser to create hierarchical surface structures.³⁷⁻³⁹ However, a large heat-affected zone and an over-melt area were generated by CW laser pulses longer than 1 ms, which reduces the textured surface structure repeatability.

Surface chemistry plays a critical role in deciding the final wettability of laser-textured metals and metal alloys. Over the years, three main surface chemistry modification strategies have been used for laser-textured metals to change the wettability to superhydrophobicity to repel water, including anchoring fluorinated groups such as perfluoroalkanes on the nanostructured surface, $^{30,40-42}_{40,43,44}$ exposing to atmospheric condition for extended periods, $^{41,43,44}_{40,43,44}$ and low-temperature heat treatment. 45 Researchers frequently used chemical treatment with fluorosilane after the surface structure generation in order to achieve superhydrophobicity for laser-textured metal alloys. ^{30,40,41,46} A monolayer of a functionalized fluorosilane reagent was coated on top of the textured surface to reduce the surface energy. Wu et al. 42 applied 97% trichloro (1H,1H,2H,2H-perfluorooctyl) silane [CF₃(CF₂)₅(CH₂)₂SiCl₃] by chemical vapor deposition (CVD) on top of the laser-fabricated microconical structure on stainless steel to achieve superhydrophobicity. Pendurthi et al. 40 applied heptadecafluoro-1,1,2,2-tetrahydrodecyl trichlorosilane [CF₃(CF₂)₇(CH₂)₂SiCl₃] after the laser texturing process on titanium, aluminum, and several stainless steels to make them superhydrophobic. During the exposing to atmospheric condition for extended periods, the laser-textured aluminum surface absorbs airborne organic molecules that lead to superhydrophobicity. 41 Adsorption of organic components

on the nanostructured surface alters the surface chemistry with enrichment of $-\mathrm{CH_2}-$ and $-\mathrm{CH_3}$ groups that contribute to superhydrophobicity. A low-temperature heat treatment process is also used before exposure to ambient air to accelerate the organic molecule adsorption, leading to superhydrophobicity. Researchers also immersed laser-textured brass in different mediums including vinegar, sodium bicarbonate solution, IPA, and salt water to study its wettability transition. IPA increased the absorption of the organic substance to accelerate wettability transition from hydrophobicity to hydrophilicity, whereas sodium bicarbonate slowed down the transition.

Similarly, two main chemistry modification strategies have been used to achieve superhydrophilicity to attract water, including anchoring the water-affinitive chemical group on the surface 48,49 and boiling water treatment. 50 The authors' research group utilized immersion treatment with a 97% 3cyanopropyltricholosilane reagent [CN(CH₂)₃SiCl₃] in ethanol solution⁴⁹ for aluminum and titanium alloys to chemically attach the polar nitrile (-CN) group on the laser-textured surfaces to achieve superhydrophilicity. Boiling water treatment also used post-laser texturing to enrich the surface micro/nanostructures with polar oxide and hydroxide groups leading to superhydrophilicity. 50 However, as the hydrophilic and superhydrophilic surfaces possessed high surface energy, they were prone to get fouled by oils and other organic matter. Those easy-fouling constituents were difficult to remove and severely affect the long-term applications of superhydrophilic surfaces.

If oil repellency or superoleophobicity can be combined with superhydrophilicity, it will provide a useful way to prevent the fouling of superhydrophilic surfaces. However, the coexistence of superhydrophilicity and superoleophobicity has never been investigated on laser-textured surfaces. It also seems unusual because the classic surface free energy (SFE) theory suggests that superoleophobic surfaces would also be superhydrophobic. Some research groups have developed stimuli-responsive surfaces by combining oleophobic -CF₂- and -CF₃ groups with the water-affinitive -C(=O)—ONa group in the same chemical structure to simultaneously display hydrophilicity and oleophobicity based on a favorable interaction with polar liquids and an unfavorable interaction with nonpolar liquids. ^{20,51-56} Yang et al. ²⁰ synthesized a complex polymer as PDDA-S-PFO, which combines poly-(diallyldimethylammonium chloride) (PDDA) as a binder with sodium perfluorooctanoate (S-PFO) [CF₃(CF₂)₆COONa]. They spray-coated a glass substrate with the PDDA-PFO polymer and SiO₂ nanoparticles to effectively achieve coexistence of superhydrophilicity and superoleophobicity. Pan et al. 52 further extended this complex polymer synthesis by producing sodium perfluorododecane (S-PFD) and copper perfluorododecane (C-PFD). They spraycoated a glass substrate and steel mesh with a mixture of titanium oxide nanoparticles, poly(vinylpyrrolidone) (PVP) as a binder, and those polymers to achieve coexistence of superhydrophilicity and superoleophobicity.

However, most of these chemistry modification techniques lack systematic theoretical guidelines for the laser surface engineering methods to achieve different wettability. A significant gap in understanding exists in the current literature to modify the surface chemistry of laser-textured metal surfaces so that the wettability can be altered for similar surface structures by changing the surface chemistry. In this work, a

methodical design approach is presented and demonstrated through experiments to modify the surface chemistry of laser-textured metal alloys to effectively alter the wettability. Three different extreme wettability scenarios, including superoleo-phobicity and superhydrophobicity, superhydrophilicity and superoleophobicity, and coexistence of superoleophobicity and superhydrophilicity, are demonstrated on the same laser-textured surface. Dual-scale microtrenches are fabricated by nanosecond laser pulses, and the laser-textured surface was further immersion-treated with different chemical functional groups. This study includes analysis of the surface structures, surface chemistry, wetting characteristics, and mechanism of achieving extreme wettabilities.

DESIGN METHODOLOGY

The design strategy to modify the surface functional group to tune extreme wettability of the same laser-textured metal alloy can be derived from Young's equation.

$$\cos \theta = \frac{\gamma_{\rm sv} - \gamma_{\rm sl}}{\gamma_{\rm lv}} \tag{1}$$

where γ_{sv} and γ_{lv} are the SFEs of solid and liquid, respectively, whereas γ_{sl} is the interface free energy at the solid–liquid interface. γ_{sl} can be expressed in terms of γ_{sv} and γ_{lv} , as demonstrated by Girifalco and Good⁵⁷

$$\gamma_{\rm sl} = \gamma_{\rm sv} + \gamma_{\rm lv} - 2\varphi \sqrt{\gamma_{\rm sv}\gamma_{\rm lv}} \tag{2}$$

where φ is the parameter describing the matching situation of molecules in solid and liquid phases. In most cases, φ is considered as 1 with negligible errors. Then, eq 1 is reduced to

$$\cos \theta = 2\sqrt{\frac{\gamma_{\rm sv}}{\gamma_{\rm lv}}} - 1 \tag{3}$$

Fowkes⁵⁸ suggested that each component of the SFE of the liquid and solid surfaces is a combination of interparticle forces that exist between nonpolar atoms or molecules and the dipole—dipole force that exists between neutral polar molecules. Therefore, total SFE had two components based on their chemical composition, i.e., dispersive $(\gamma^{\rm d})$ and nondispersive $(\gamma^{\rm n})$, which were attributed to the dispersion force component and hydrogen bonding/dipole—dipole interaction, respectively. Therefore

$$\gamma_{\rm sv} = \gamma_{\rm sv}^{\rm d} + \gamma_{\rm sv}^{\rm n} \tag{4}$$

$$\gamma_{lv} = \gamma_{lv}^d + \gamma_{lv}^n \tag{5}$$

where γ^d_{sv} and γ^n_{sv} are the dispersive and nondispersive components of the SFE of the solid surface whereas, γ^d_{lv} and γ^n_{lv} are the dispersive and nondispersive components of SFE of the liquid.

Depending on the processing condition of the solid surface, the dispersive and nondispersive components of the processed solid surface can be controlled to decide the final equilibrium wetting condition. Then, eq 2 can have a more generic form

$$\gamma_{\rm sl} = \gamma_{\rm sv} + \gamma_{\rm lv} - 2\sqrt{\gamma_{\rm sv}^{\rm d}\gamma_{\rm lv}^{\rm d}} - 2\sqrt{\gamma_{\rm sv}^{\rm n}\gamma_{\rm lv}^{\rm n}}$$
 (6)

Then, from Young's equation, θ can be expressed in a more generic form

$$\cos \theta = \frac{2\sqrt{\gamma_{sv}^d \gamma_{lv}^d} + 2\sqrt{\gamma_{sv}^n \gamma_{lv}^n}}{\gamma_{lv}^d + \gamma_{lv}^n} - 1$$
(7)

Water contains both dispersive and nondispersive components. Therefore, the $\theta_{\rm w}$ can be expressed as

$$\theta_{w} = \cos^{-1} \left[\frac{2\sqrt{\gamma_{sv}^{d}} \gamma_{lv}^{d} + 2\sqrt{\gamma_{sv}^{n}} \gamma_{lv}^{n}}{\gamma_{lv}^{d} + \gamma_{lv}^{n}} - 1 \right]$$
(8)

On the other hand, γ_{lv}^n is negligible for oils as they are generally nonpolar; therefore, oil contact angle (θ_o) can be expressed as

$$\theta_{o} = \cos^{-1} \left[\frac{2\sqrt{\gamma_{sv}^{d}\gamma_{lv}^{d}}}{\gamma_{lv}^{d}} - 1 \right]$$
(9)

Based on this theory, the design approach is developed to achieve superhydrophobicity, superhydrophilicity, and coexistence of superoleophobicity and superhydrophilicity. The surface functional groups are chosen in such a way that three different scenarios of chemical composition can be attained, as shown in Figure 1. For case I, chemical composition with

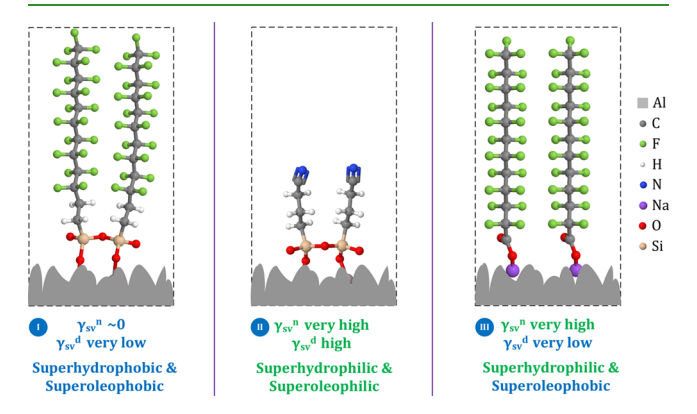


Figure 1. Designs of surface chemistry with various dispersive and nondispersive components.

 $-CH_2-$, $-CF_2-$, and $-CF_3$ groups is known to be a very balanced chemical configuration with γ^n_{sv} being zero as there are no polar groups on the solid surface and γ^d_{sv} is very low. The critical surface tension of those groups, as listed in Table 1,

Table 1. Critical Surface Tension of Low-Energy Chemical Groups 59

ranks those groups according to their critical surface tension. It indicates that fluorocarbon groups induce lower SFE conditions compared to alkyl groups. In general, SFE of oil is lower than water ($\gamma_{\rm ov} < \gamma_{\rm wv}$); therefore, θ of oil is lower than water ($\theta_{\rm o} < \theta_{\rm w}$). For a specific solid surface with $-{\rm CF_2}-$ and $-{\rm CF_3}$ groups, if the surface is proved to be oleophobic, then it would be hydrophobic.

For case II, surface chemistry was chosen to be the nitrile $(-C \equiv N)$ group, which possesses a highly electronegative

Table 2. Average Dipole Moment of Polar Chemical Groups 60,61

chemical groups	nitrile	amide	ketone	aldehyde	carboxyl	ester
degree of polarity (Debye)	3.9	3.76	2.88	2.72	1.74	1.72

Table 3. List of Chemicals Used for Immersion Treatment

name	acronym	chemical formula	
1H,1H,2H,2H-perfluorooctyltrichlorosilane	FOTS	$[CF_3(CF_2)_5(CH_2)_2SiCl_3; 98\%]$	
1H,1H,2H,2H-perfluorodecyltrichlorosilane	FDTS	$[CF_3(CF_2)_7(CH_2)_2SiCl_3; 97\%]$	
1H,1H,2H,2H-perfluorododecyltrichlorosilane	FDDTS	$[CF_3(CF_2)_9(CH_2)_2SiCl_3; 97\%]$	
3-cyanopropyltricholosilane	CPTS	[CN(CH2)3SiCl3; 97%]	
perfluorododecanoic acid	A-PFDD	[CF ₃ (CF ₂) ₁₀ COOH; 92%]	
poly(vinylpyrrolidone)	PVP	$[(C_6H_9NO)_n; 99.5\%; powder]$	
anhydrous sodium acetate		[CH ₃ COONa; 99.4%; crystal]	

nitrogen atom that makes the functional group highly polar. The nitrile group is selected in this study as it has the highest degree of polarity among the polar chemical groups, as listed in Table 2. Therefore, the treated surface has a very high nondispersive $\gamma_{\rm sv}^{\rm n}$ component. The surface does not contain a long chain of fluorocarbon or alkyl group; therefore, $\gamma_{\rm sv}^{\rm d}$ is not low. Now, as the $\gamma_{\rm sv}^{\rm d}$ component is very high in this case, the right side of eq 8 lies between 0 and 1, resulting in a hydrophilic surface. Again, as $\gamma_{\rm sv}^{\rm d}$ is also relatively high and surface tension of oils is low, the treated surface is expected to behave as oleophilic as well.

For case III, the chemical condition is chosen to be a combination of both low energy $-CF_2-$ and $-CF_3$ groups and the highly polar (-COONa) group. Therefore, the surface contains a very low dispersive component and a very high nondispersive component. Now, in general, the SFE of oil is lower than water ($\gamma_{\rm ov} < \gamma_{\rm wv}$). Therefore, from eqs 8 and 9, θ of oil is lower than water ($\theta_{\rm o} > \theta_{\rm w}$). For a specific solid surface with both low energy $-CF_2-$ and $-CF_3$ groups and the highly polar (-COONa) group, the surface can behave as both oleophobic and hydrophilic.

Textured surfaces possess roughness, which is not considered in the above derivation. Due to the presence of surface roughness, the θ measurement by Young's model is different from the actual θ . According to Wenzel's mode, ⁶² the real surface area increased due to the presence of surface roughness and the apparent contact angle (θ^*) can be expressed as

$$\cos(\theta^*) = r_f \frac{\gamma_{sv} - \gamma_{sl}}{\gamma_{lv}} = r_f \cos(\theta)$$
(10)

where $r_{\rm f}$ ($r_{\rm f} > 1$) is the solid surface roughness factor, which signifies the ratio of solid surface area to the projected area. Therefore, the $\theta_{\rm w}$ and $\theta_{\rm o}$ from eqs 8 and 9 can be expressed as

$$\theta_{w}^{*} = \cos^{-1} \left[r_{f} \left(\frac{\sqrt[2]{\gamma_{sv}^{d} \gamma_{lv}^{d} + \sqrt[2]{\gamma_{sv}^{n} \gamma_{lv}^{n}}}}{\gamma_{lv}^{d} \gamma_{lv}^{n}} - 1 \right) \right]$$

$$(11)$$

$$\theta_{o}^{*} = \cos^{-1} \left[r_{f} \left(\frac{\sqrt[2]{\gamma_{sv}^{d} \gamma_{lv}^{d}}}{\gamma_{lv}^{d}} - 1 \right) \right]$$
(12)

Therefore, from eqs 11 and 12, both hydrophobicity and hydrophilicity are improved further in the presence of surface roughness.

Cassie and Baxter⁶³ introduced a composite contact model where liquid droplets did not move inside the surface roughness. Some gas is trapped in between the liquid and solid. Therefore, the solid–liquid interface is a combination of the solid–liquid and solid–gas interfaces and only a fraction of r_f (0 < f < 1) contributed toward the solid–liquid interface. After introducing the roughness factor into the Cassie–Baxter model, the apparent contact angle (θ^{**}) can be given as

$$\cos(\theta^{**}) = r_f f \cos(\theta) + f - 1 \tag{13}$$

Therefore, the $\theta_{\rm w}$ and $\theta_{\rm o}$ can be expressed as

$$\theta_{w}^{**} = \cos^{-1} \left[r_{f} f \left(\frac{\sqrt[2]{\gamma_{sv}^{d} \gamma_{lv}^{d} + \sqrt[2]{\gamma_{sv}^{n} \gamma_{lv}^{n}}}}{\gamma_{lv}^{d} \gamma_{lv}^{n}} - 1 \right) + f - 1 \right]$$
(14)

$$\theta_{o}^{**} = \cos^{-1} \left[r_{f} \left(\frac{\sqrt[2]{\gamma_{sv}^{d} \gamma_{lv}^{d}}}{\gamma_{lv}^{d}} - 1 \right) + f - 1 \right]$$
(15)

Therefore, from eqs 14 and 15, surface roughness improves hydrophobicity and oleophobicity further when the liquid droplet does not penetrate the roughness.

EXPERIMENTS

nHSN Process for Surface Fabrication and Chemistry Modification. The author's group 48,64 has developed a unique nanosecond laser-based high-throughput surface nanostructuring (nHSN) process using a nanosecond laser for metal alloys to texture metal alloys for wettability modification. Previously, they have applied this process to achieve superhydrophobicity. 65,66 This nHSN process involved two sequential steps: (a) nanosecond laser texturing in air (aNLT) during which the AA6061 surface was irradiated with a nanosecond pulse laser and (2) chemical immersion treatment (CIT) during which the laser-treated surface was immersed in a chemical solution to attach the chemical functional group on the textured surface. In this study, AA6061, procured from McMaster-Carr, USA, is used as the substrate material. AA6061 samples were ultrasonically cleaned in acetone, ethanol, and deionized (DI) water for 15 min successively. The samples were subsequently rinsed in DI water for 15 s and dried at room temperature for 24 h.

The laser texturing setup consisted of a Nd:YAG nanosecond laser, a galvanometer laser scanner, several mirrors, a cooling system to cool down the laser scanner during experiments, an XYZ stage to hold the workpiece, and a computer with a microcontroller. More detail about the process setup can be found in the work of Samanta et al.⁶⁷ During the laser texturing, the laser beam was Gaussian in nature, the pulse width was kept as 120 ns, and the experiments were performed at ambient conditions. A 0.6 W laser power was used, and the laser beam

Table 4. Chemical Solution Preparation for the CIT Process

designed wettability case I: superhydrophobicity and superoleophobicity

chemical solution for the CIT process 0.25 g of solid FDDTS/1.5 mL of FDTS/1.5 mL 1.5 mL of CPTS + 98.5 mL of FOTS + 100 mL of absolute toluene of absolute ethanol

case II: superhydrophilicity and superoleophilicity

case III: coexistence of superhydrophilicity and superoleophobicity

6.7 g of A-PFDD + 100 mL of absolute ethanol + 0.82 g of anhydrous sodium acetate + 0.2 g of PVP

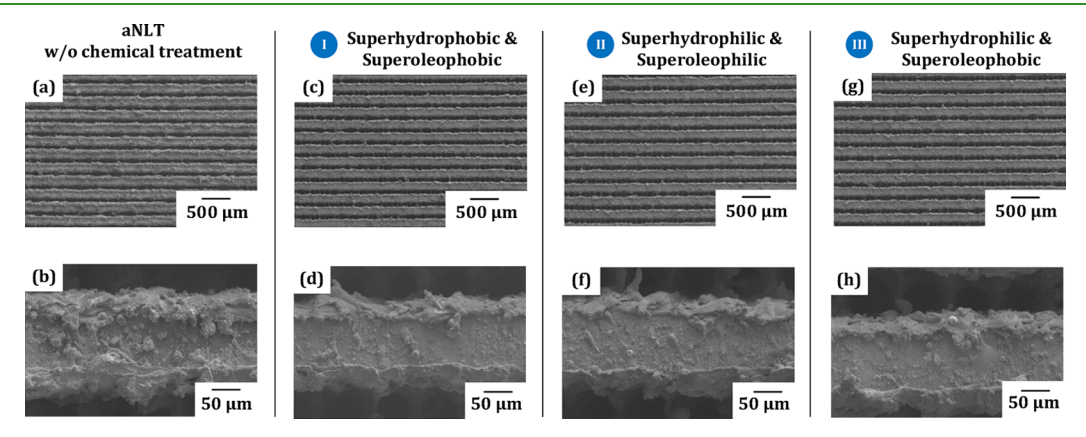


Figure 2. Comparison of the surface structure on AA6061 at low and high magnifications for (a, b) only aNLT-treated, (c, d) superhydrophobic and superoleophobic, (e, f) superhydrophilic and superoleophobic, and (g, h) coexistence of superhydrophilicity and superoleophobicity.

diameter was kept as $\sim 100~\mu m$ (see the Supporting Information, Section S1). The laser scanner irradiated the workpiece top surface in a predesigned zig-zag pattern. The laser scanning was selective, which means that some area was textured, whereas some area was left untextured.

After the aNLT process, the textured AA6061 specimens were immersed in different chemical solutions at room temperature for 3 h during the CIT process to achieve the designed wettability scenarios. Chemical reagents, as listed in Table 3, were obtained from Alfa Aesar and Sigma-Aldrich for chemical treatment. Ethanol (C₂H₅OH; 99.5%) and toluene (C₆H₅CH₃; 99.8%), procured from Sigma-Aldrich, are used as solvents to prepare the solution for chemical treatment. The chemical solutions used to achieve different wettabilities are listed in Table 4. All the solutions were stirred for 30 min in a magnetic stirrer at room temperature to assure a uniform mixture. Details of the preparation of each chemical solution can be found in the Supporting Information, Section S2. After 3 h, the specimens were taken out of the solution and cleaned with DI water and subsequently dried using compressed air. After that, specimens were dried in a vacuum oven at 80 °C for 1 h.

Post-Process Characterizations. Morphology of the laser-irradiated and chemical-treated rough samples was analyzed using scanning electron microscopy (SEM; Hitachi S-4800). Surface chemical composition was obtained using a Kratos Axis ultrahigh-performance X-ray photoelectron spectroscopy (XPS) system using an Al K α (1486.6 eV) line excitation source. Both survey spectrum analysis and core-level spectrum analysis were performed. Before and after the CIT process, chemical analysis was performed using inductively coupled plasma-optical emission spectroscopy (ICP-OES) to analyze the trace of the substrate material into the chemical solution. The dynamic spreading of the water droplet on the superhydrophilic surfaces was measured using a high-speed imaging system (PCO Tech, Dimax) using a high-magnification 12× zoom lens system (LaVision). The images were captured at 1000 frames/s to trace the spreading of a water droplet.

Contact angle measurements were performed using a Rame-Hart model 100 contact angle goniometer at ambient temperatures. Four different liquids including, DI water, glycerol ($C_3H_8O_3$; 99.5%), diiodomethane (CH_2I_2 ; 99%), and ethylene glycol ($OH(CH_2)_2OH$; 99.8%) were procured from Sigma-Aldrich and employed for wettability testing. During the θ measurement for those liquids, 4 μ L of liquid droplet was micropipetted on the treated surface. For each specimen, six θ measurements were obtained at different locations, and the average value is reported. Liquid droplet roll-off

tests for superhydrophobic and superoleophobic samples were conducted using an in-house designed roll-off angle ($\theta_{\rm roll-off}$) measurement apparatus, which consisted of a rotable stage to hold the nHSN-treated surface horizontally and tilted the stage with a resolution of 0.1°. For each $\theta_{\rm roll-off}$ measurement, a 4 μ L of liquid droplet was micropipetted onto the treated surface, and the stage started rotating until the water droplet rolled off the surface. The critical angle that the liquid droplet began to slide down on the inclined stage was recorded as the $\theta_{\rm roll-off}$.

■ RESULTS AND DISCUSSION

Dual-Scale Surface Morphology. In this study, the identical laser processing condition was applied across all three case studies to keep the surface topography similar. Microtrenches have been fabricated using the nHSN process with process parameters. Figure 2a shows SEM images of that the processed surface consisted of multiple parallel microtrenches with a width of $\sim 100 \ \mu m$ and a period of $\sim 250 \ \mu m$ after the aNLT process step. Those microtrenches were formed by connecting a series of blind holes ablated by laser pulses. The higher magnification SEM micrograph (Figure 2b) shows that the ridges of the microtrenches were covered with burrs. The burrs were formed by the redeposition of the ablated material around the edges of the microtrenches. This burr formation was not suitable for conventional products, but it was essential for surfaces with extreme wettabilities. The SEM micrographs were also analyzed after the CIT process for all the three kinds of extreme wettabilities achieved in this study, i.e., superoleophobicity and superhydrophobicity, superhydrophilicity, and coexistence of superhydrophilicity and superoleophobicity. Figure 2c-h demonstrates surface morphologies for all three wettability conditions. Dual-scale surface morphologies with microtrenches covered with micro/nanoscale burrs/ripples/ protrusions were observed. This indicates that the microstructures were similar for all the three wettability conditions.

Design and Processing Mechanism for Case I: Superhydrophobicity and Superoleophobicity. The designing intent of creating superoleophobic and superhydrophobic AA6061 was to anchor the fluorocarbon chain on top of the dual-scale surface structures created by the aNLT

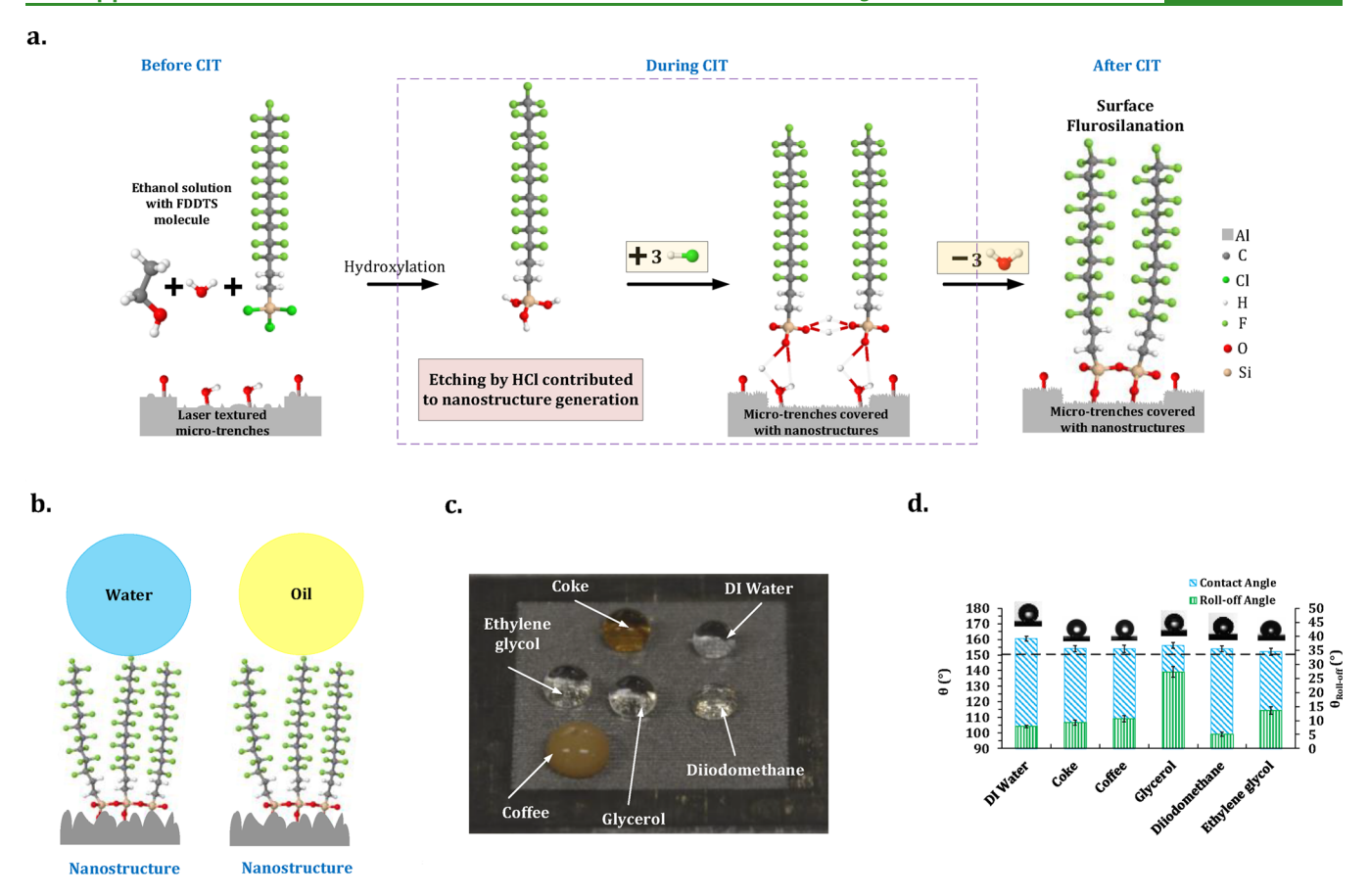


Figure 3. Designing a superoleophobic/superhydrophobic surface. (a) Schematic representation of the mechanism of attachment of FDDTS molecules on the laser-textured surface during the CIT process. (b) Attached FDDTS molecule shows low dispersive and nondispersive parts of the solid SFE, thus repelling both oil and water. (c) Different liquids formed spherical droplets on the treated surface. (d) θ and $\theta_{\text{roll-off}}$ of different laboratory solvents and liquids from daily life.

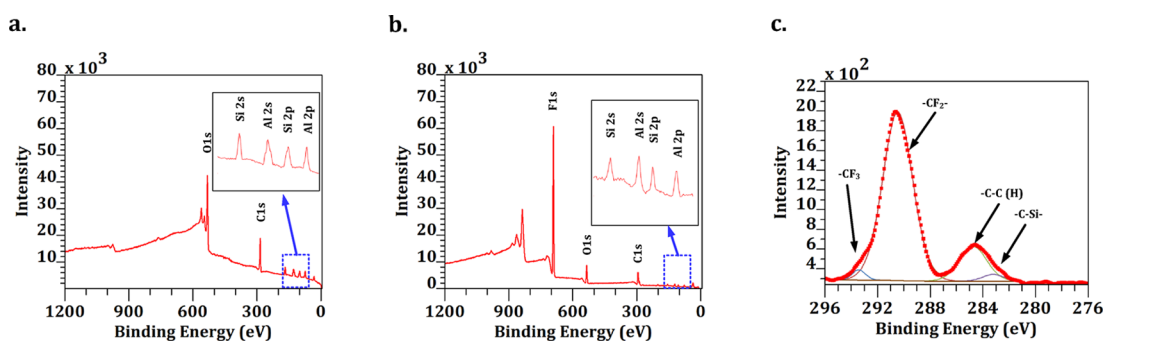


Figure 4. Surface chemistry at different stages of producing the superoleophobic/superhydrophobic AA6061 surface. (a) XPS survey analysis after the aNLT process. (b) XPS survey analysis after the CIT process with the FDDTS reagent. (c) Core-level analysis of C 1s.

step. The target processing intent was achieved as a combination of aNLT and CIT processes. The aNLT process created parallel microtrenches covered with randomly distributed micro/nanoscale structures on the AA6061 surface, and the CIT process attached FDDTS molecules in the peaks and valleys of microtrenches. The mechanism of chemical attachment of FDDTS molecules on the processed surface is hypothesized in Figure 3a. The FDDTS reagent consisted of two distinct groups, i.e., the reactive group, which includes $-\text{SiCl}_3$, and the functional group, which provided for $-(\text{CH}_2)_2(\text{CF}_2)_9\text{CF}_3$. During the CIT process, chlorine atoms of the reactive group were replaced by -OH through hydroxylation, and HCl was generated during the intermediate

chemical reaction of fluorosilane molecules. Each FDDTS molecule produced three molecules of HCl during the process. HCl contributed to etch some of the AA6061 as aluminum chloride (AlCl₃) during the CIT process. The etching effect enhanced the nanostructure generation on the surface (see the Supporting Information, Section S3).⁴⁸ Simultaneously, the FDDTS molecule linked with surface hydroxide of the laser-treated surface and got itself anchored by releasing three molecules of water.

Attachment of the FDDTS molecule led to surface fluorination resulting in very low dispersive and nondispersive parts of the solid SFE. Consequently, the treated surface can repel both oil and water, as shown in Figure 3b. Liquids in

water and oil category, i.e., water, coffee, coke, glycerol, diiodomethane, and ethylene glycol, have been tested on the treated surface, and they formed spherical droplets on the surface, as shown in Figure 3c. The θ for all the liquids is more than 150°, as shown in Figure 3d. To further validate the superoleophobicity achieved on treated AA6061 surfaces, the $\theta_{\rm roll-off}$ of all the above-mentioned liquids was measured. The experimental results demonstrate that the $\theta_{\rm roll-off}$ for water, coffee, and coke are between 8–11° with an uncertainty of 0.8°. The $\theta_{\rm roll-off}$ of diiodomethane, glycerol, and ethylene glycol are consistently less than 30°. Both water and diiodomethane droplets rolled off the surface immediately after coming into contact with the processed superoleophobic and superhydrophobic surface (see Movie S1).

The surface chemistry of the superoleophobic and only laser-treated AA6061 surface was investigated by XPS analysis, as shown in Figure 4. It can be observed that immediately after aNLT, the AA6061 surface contains Al, O, C, and Si. The origin of Al and Si belonged to the composition of AA6061, and O came from the oxidation/hydroxylation that occurred during the aNLT process (Figure 4a). C came from adsorption of biomolecules on the treated surface in between the surface preparation and XPS analysis. After the completion of the CIT process with FDDTS, F was detected along with previous peaks (Figure 4b). The F and Si peaks belonged to the FDDTS reagent $[CF_3(CF_2)_9(CH_2)_2SiCl_3]$. Detailed core-level analysis of the C 1s peak was performed based on the binding energy of different carbon-related chemical groups, as listed in Table 5.

Table 5. List of Binding Energies of Different Chemical Functional Groups in C $1s^{69-74}$

carbon compounds	binding energy (eV)
-С-С-, -С-Н	284.7-285.3
-CF ₃	293.5-293.8
-CF ₂ -	292.5-293.2
-C-Si-	281.8-283.2
-CN	286.0-286.5
-C(=0)-0-	289.0-289.1

The study shows that the C 1s peak was a combination of the $-\mathrm{CH_2}$ -, $-\mathrm{CF_2}$ -, and $-\mathrm{CF_3}$ chemical groups (Figure 4c). It also shows the presence of $-\mathrm{Si-C-}$ at 283.1 eV. Those functional groups were present on the FDDTS structure, which indicates that the FDDTS molecules were successfully attached to the laser-textured surface after the CIT process, leading to surface fluorination. Surface fluorination led to a reduction in

SFE^{68,69} of the textured solid surface resulting in superoleophobicity. The absence of the Cl peak in the XPS survey spectrum also confirmed the occurrence of the chemical etching event during the CIT process that dissolved some part of the AA6061 substrate as aluminum chloride in the solution.

Effect of Fluorocarbon Chain Length. The effects of length of the fluorosilane reagents were also studied in this work. Three different fluorosilanes were used, including FOTS, FDTS, and FDDTS. The difference between three fluorosilane reagents was the length of the -CF₂- chain in the functional group in their chemical structure. The lengths of -CF₂groups for FOTS, FDTS, and FDDTS were five, seven, and nine, respectively. The comparison of the θ for water and diiodomethane is shown in Figure 5a. The θ is above 150° for both liquids; however, the θ value was increased when the length of the functional group was increased. $\theta_{\text{roll-off}}$ was also compared, as shown in Figure 5b. Increasing the length of the $-CF_2$ - group resulted in lower $\theta_{roll-off}$ for both water and diiodomethane. Increasing the length of fluorosilane put more -CF₂- groups on the laser-treated surface, as confirmed by XPS analysis (Figure 5c). More $-CF_2$ — on the processed surface led to a lower dispersive component of SFE, resulting in lower $\theta_{\text{roll-off}}$ and higher θ . These experimental results clearly illustrated the influence of the length of the functional group on the surface superhydrophobicity and superoleophobicity. An increase in the silane tail group length improved both superhydrophobicity and superoleophobicity for similar surface microstructures.

Design and Processing Mechanism for Case II: Superhydrophilicity and Superoleophilicity. The designing intent of creating superhydrophilic AA6061 was to attach a highly polar nitrile (—C≡N) group on top of laser-textured dual-scale surface structures. It was achieved by immersion treatment of laser-textured AA6061 specimens with the CPTS reagent during the CIT process. The mechanism of chemical attachment of CPTS molecules on top of laser-irradiated structures is presented in Figure 6a. The reactive part of the CPTS molecules (-SiCl₃) is the same as the silanes used to make the superoleophobic surface in the Design and Processing Mechanism for Case I: Superhydrophobicity and Superoleophobicity section . Therefore, the chemical reaction for attachment of the CPTS molecules was similar. During the CIT process, both chemical etching and attachment of the functional group happened simultaneously. During the chemical event, HCl was also generated by hydroxylation of CPTS molecules leading to surface chemical etching. After the attachment of CPTS molecules to the textured surface, the

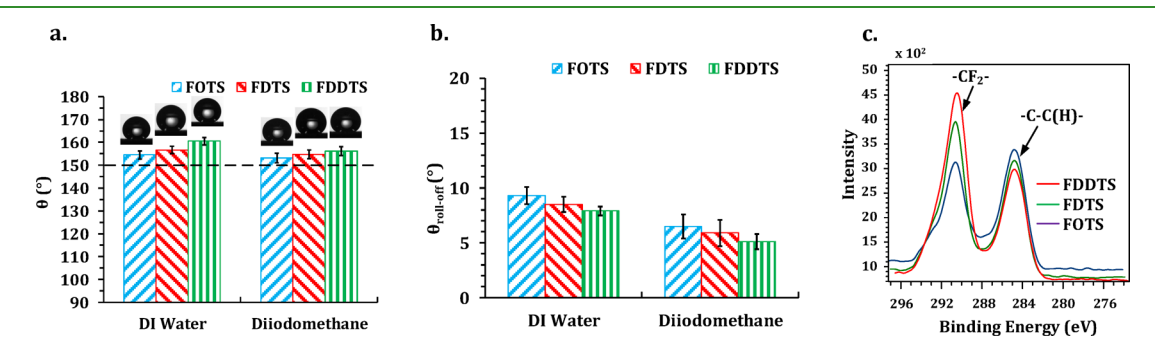


Figure 5. Variation of superoleophobicity and superhydrophobicity depending on fluorosilane chemistry. (a) Variation of θ of water and diiodomethane on surfaces depending on the length of the fluorocarbon chain. (b) Variation of $\theta_{\text{roll-off}}$ of water and diiodomethane on surfaces depending on the length of the fluorocarbon chain. (c) Core-level analysis of C 1s for surfaces treated with different lengths of fluorocarbon chain.

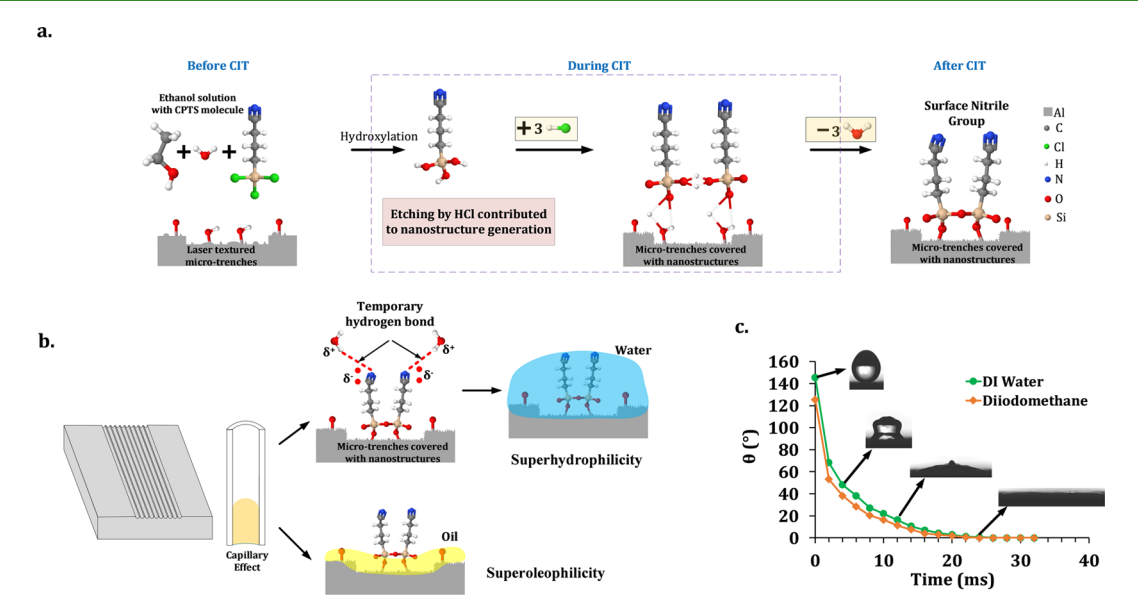


Figure 6. Designing a superhydrophilic and superoleophilic AA6061 surface. (a) Schematic representation of the mechanism of attachment of CPTS molecules on the laser-textured surface during the CIT process. (b) Combination of temporary hydrogen bond formation and capillary effect leading to superhydrophilicity and superoleophilicity. (c) Spreading of a water and diiodomethane droplets on the treated surface.

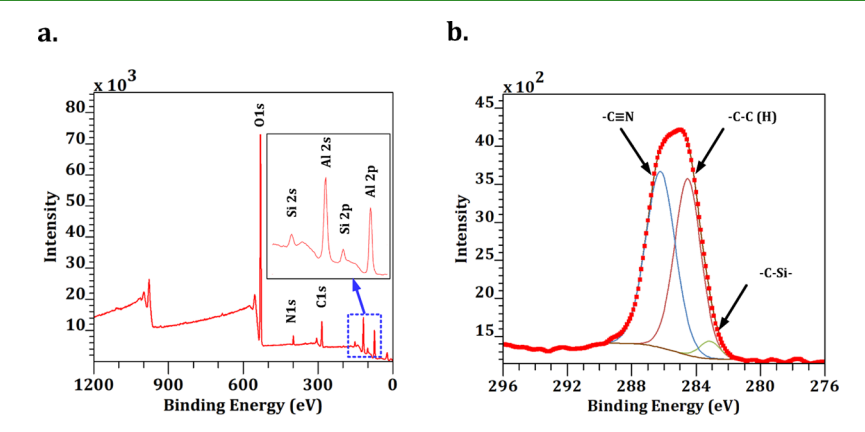


Figure 7. XPS analysis of the surface layer for AA6061 with superhydrophilicity and superoleophilicity. (a) Survey analysis after the CIT process. (b) Core-level analysis of C 1s.

functional nitrile group was aligned outward from the treated surface.

CPTS molecules contained a nitrile group, which was highly polar due to the triple covalent bond of carbon with highly electronegative nitrogen. Nitrogen pulled the electrons of the —C≡N bond toward itself and induced polarity. On the other hand, water was a polar molecule due to the presence of highly electronegative oxygen. The oxygen atom drew electrons toward itself, making the regions around two hydrogen atoms more positive than the area around itself. It resulted in H⁺ and OH groups inside each water molecule. The slightly positive hydrogen atom in a water molecule was drawn toward the slightly negative nitrogen atom in the surface nitrile group, and a temporary hydrogen bond was formed, as schematically illustrated in Figure 6b. The treated surface contained a monolayer of CPTS molecules on top of the surface structures. The resultant hydrogen bonding and dipole-dipole attraction contributed toward superhydrophilicity. Surfaces with dualscale structures with water-affinitive chemistry were known to enhance superhydrophilicity by allowing a liquid trail through the higher scale trenches, whereas the capillary pressure was maintained at the comparatively lower scale structures. Water droplets spread immediately at a very fast rate after coming into contact with superhydrophilic surfaces (see Movie S2). As the surface chemistry does not have long-chain hydrocarbon or fluorocarbon, the dispersive component of the SFE is also relatively high. On the other hand, diiodomethane has low surface tension compared to water. Therefore, diiodomethane also spread on the surface effectively (see Movie S2). To elucidate the dynamic wetting effect on the treated surface over time, a deionized water droplet and a diiodomethane droplet with 5 μ L volume were dropped on the processed surface, and the evolution of droplet spreading is captured as a function of time using a high-speed camera. The liquid front propagated through the dual-scale structure resulting in a rapid spreading, as shown in Figure 6c. Apart from surface polarity, the treated surface has a strong capillary effect due to the presence of microtrenches.⁷⁵ Therefore, they can draw the water and diiodomethane molecules very fast through the surface hierarchical structures. Superhydrophilicity is additionally attributed to the capability of hydrogen bond formation with the polar nitrile group (Figure 6b).

The surface chemistry of the superhydrophilic AA6061 surface was characterized by XPS analysis. XPS survey

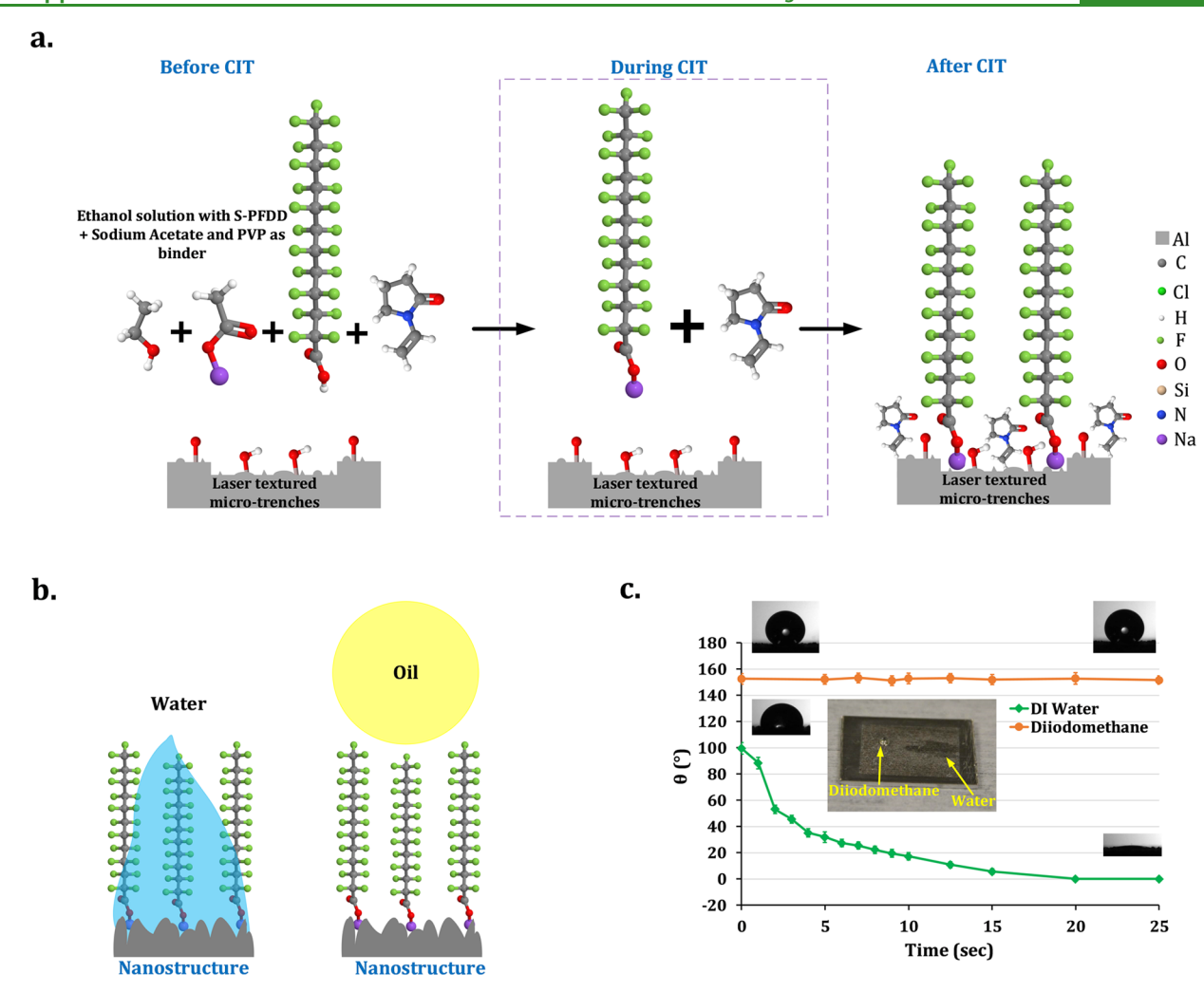


Figure 8. Designing a AA6061 surface with coexistence of superoleophobicity and superhydrophilicity. (a) Schematic representation of the mechanism of attachment of S-PFDD molecules on the laser-textured surface during the CIT process. (b) Attached S-PFDD molecule shows low dispersive and high nondispersive parts of the solid SFE, thus attracting water and repelling oil. (c) Spreading of a water droplet on the treated surface and retaining of diiodomethane in droplet form.

spectrum shows the presence of Al, Si, C, N, and O on the surface (Figure 7a). The intensity peaks of Al and Si came from the composition of AA6061, and the O peak was attributed to the surface oxidation during the aNLT process. C, N, and Si peaks belonged to CPTS reagent. Detailed core-level analysis shows that the C 1s peak was a result of $-CH_2-$, -CN, and -C-Si- peaks (Figure 7b). This XPS analysis confirmed the successful attachment of the CPTS molecule on the surface.

Design and Processing Mechanism for Case III: Coexistence of Superhydrophilicity and Superoleophobicity. The designing intent of creating an AA6061 surface with the coexistence of superoleophobicity and superhydrophilicity was to attach the fluorocarbon chain as well as the polar —COONa group in the same chemical structure on top of the dual-scale surface morphology created by the aNLT step. The mechanism of chemical attachment of sodium perfluorododecanoate (S-PFDD) molecules on the processed surface during the CIT process is shown in Figure 8a. During the process, sodium acetate reacted with A-PFDD and created S-PFDD. Unlike the superoleophobic and superhydrophilic scenarios, there was no reaction between the S-PFDD and the AA6061 substrate. Therefore, an external binder, PVP, was

used to anchor the S-PFDD molecules to the substrate. Once the ethanol solvent dried up, the PVP firmly attaches the S-PFDD on top of the laser-treated surface structures.

The S-PFDD contained -CF₂- and -CF₃ groups that led to a low dispersive component of solid surface energy. It also contained a highly polar sodium carboxylate group (-COONa), which comprised of highly electronegative oxygen and highly electropositive sodium. As a result, the treated surface had a very high nondispersive component of solid surface energy. Due to the presence of low dispersive and high nondispersive components, the surface behaved as superoleophobic and superhydrophilic simultaneously, as demonstrated schematically in Figure 8b. Droplets (4 μ L) of water and diiodomethane were introduced on the treated surface. When 4 µL droplets of water and diiodomethane were introduced into the tilted surface, the water droplet stretched immediately after contact, whereas the diiodomethane droplet rolled off the surface (see Movie S3). Photos of diiodomethane and water droplets are shown in Figure 8c. The treated surface showed good repellence to diiodomethane while the water wetted the surface. Diiodomethane forms a spherical droplet on the treated surface, whereas water spread on the surface.

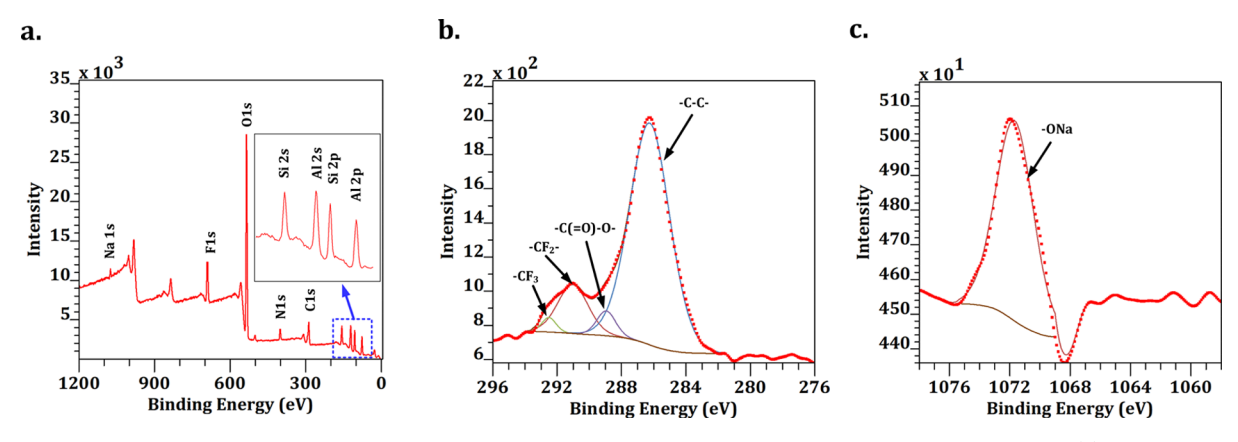


Figure 9. XPS analysis of the surface layer for AA6061 with coexistence of superoleophobicity and superhydrophilicity. (a) Survey analysis. (b) Core-level analysis of C 1s. (c) Core-level analysis of Na 1s.

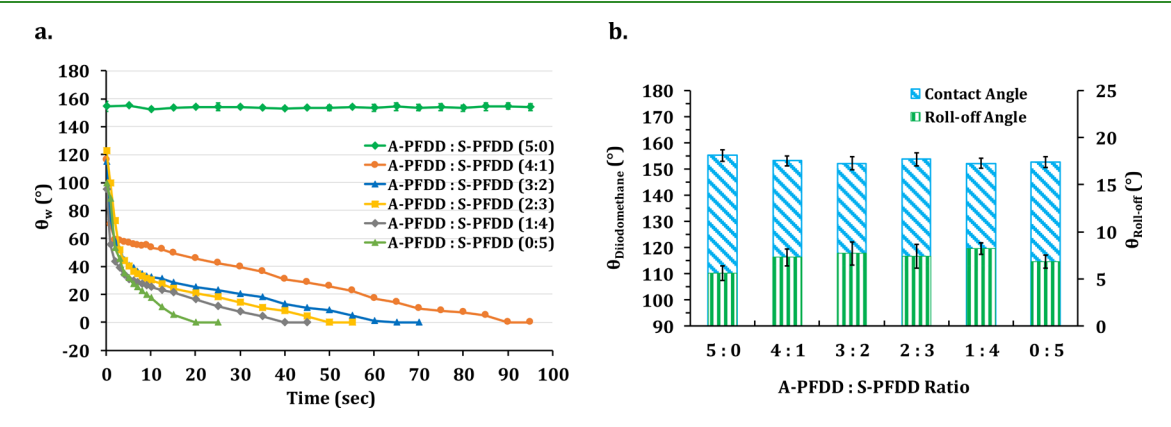


Figure 10. Wetting behaviors of water and diiodomethane on laser-textured surfaces with different A-PFDD/S-PFDD ratios from 5:0 to 0:5. (a) Variation of θ_w with time. (b) Contact angle and roll-off angle of diiodomethane.

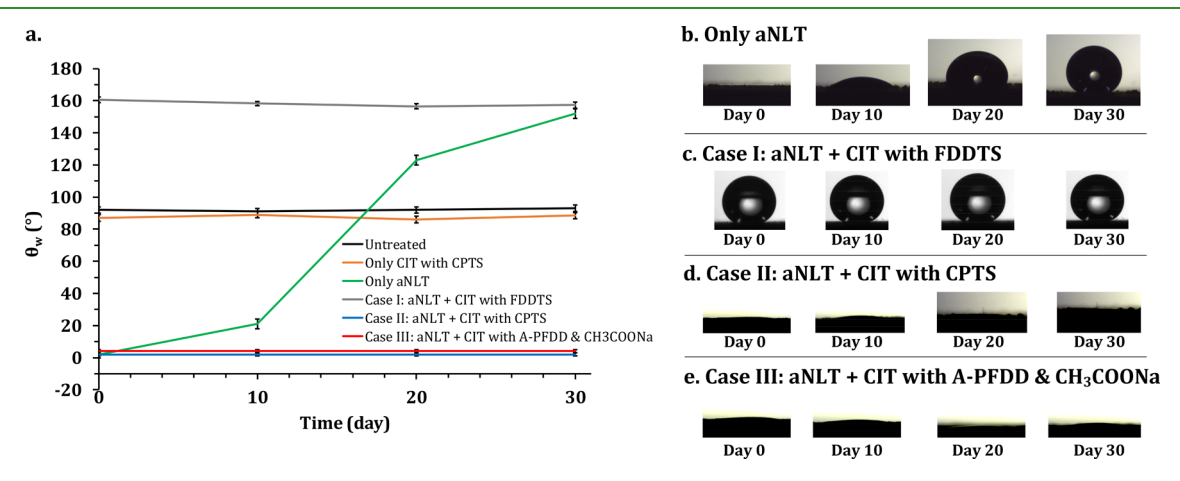


Figure 11. Progression of wettability of AA6061 surfaces with time: (a) for different combinations of aNLT and CIT processes, (b) only aNLT, (c) aNLT + CIT with FDDTS, (d) aNLT + CIT with CPTS, and (e) aNLT + CIT with A-PFDD and CH₃COONa.

The $\theta_{\rm diiodomethane}$ was consistently above 150° whereas the $\theta_{\rm w}$ drops down from 100 to 0° within 20 s.

The XPS survey analysis shows that the surface contains Al, Si, C, N, O, F, and Na (Figure 9a). The source of Al and Si intensity peaks belongs to the composition of AA6061. The source of the F and Na belonged to the S-PFDD reagent $[CF_3(CF_2)_{10}COONa]$. O comes from laser texturing, as well as the S-PFDD molecules. N was coming from the PVP binder. Core-level analysis of the carbon element shows that the carbon peak was a combination of the $-CF_2-$ and $-CF_3$,

-COO-, and -C-C- chemical groups (Figure 9b). Further, the core-level analysis of the sodium element confirmed the presence of the -COONa group, as illustrated in Figure 9c. Thus, it can be concluded that S-PFDD molecules were bound on the treated surface by PVP.

Wetting Behaviors with Different Dispersive and Nondispersive SFE Components. The evolution of $\theta_{\rm w}$ was measured on treated surfaces with different A-PFDD/S-PFDD ratios, as shown in Figure 10a. A-PFDD/S-PFDD ratio was varied from 5:0 to 0:5 across six samples processed with the

same aNLT process condition. With only A-PFDD on the surface, the $\theta_{\rm w}$ remained above 150°. The $\theta_{\rm w}$ dropped down to 0° when the A-PFDD/S-PFDD was decreased. The rate of θ_{w} dropping increased when the A-PFDD/S-PFDD was decreased from 4:1 to 0:5. When the surface was treated with only A-PFDD, the treated surface contained only the dispersive component leading to superhydrophobicity. However, with the increase in the A-PFDD/S-PFDD ratio, the nondispersive component of the solid SFE started to increase, resulting in a gradual stretching and spreading of the water droplet. On the other hand, $\theta_{\rm diiodomethane}$ remained above 150° for all the A-PFDD/S-PFDD ratios, as illustrated in Figure 10b. The $\theta_{\text{roll-off}}$ of the diiodomethane remained less than 10° for all the A-PFDD/S-PFDD ratios. As the wetting interaction of diiodomethane was only dependent on the dispersive components of the solid SFE, there was no obvious change in $heta_{
m diiodomethane}$ due to constant dispersive components for all the A-PFDD/S-PFDD ratios. These results firmly supported the proposed design principle for the coexistence of superhydrophilicity and superoleophobicity.

Stability of nHSN Surface Wettability. The untreated surface had a $\theta_{\rm w}$ of 92° \pm 0.5°, and it was very stable over a 30 day period in air. On the other hand, the wettability condition of the only aNLT-treated surface was not constant. Immediately after the aNLT process, the treated surface performed as superhydrophilic with $\theta_{\rm w} = 0^{\circ}$. Upon exposure to ambient conditions, the wettability underwent a transition from hydrophilicity to hydrophobicity as a function of time, as shown in Figure 11a. The contact angle becomes 152° within 30 days (Figure 11b). Similar wettability transition was observed by other researchers for several engineering materials including stainless steel, 44,76 aluminum alloys, 33,44 titanium alloys, 77 copper, 78 brass, 35,79 and inconel. 80 The transition time usually varies from 10 to 30 days. As laser processing of metal in air is a high-energy processing, it generates high temperatures locally. As a result, the textured metal reacts with atmospheric oxygen and generates metal oxide on the textured surface. Metal oxides are typically hydrophilic because their electronic structure favors the formation of hydrogen bonds.⁸ Metal oxides possess higher surface energy. For instance, immediately after laser treatment, the AA6061 surface contains Al_2O_3 and the surface aluminum atoms form hydrogen bonds with interfacial water molecules due to electron deficiency. 82,83 The presence of those unsaturated oxide polar sites resulted in hydrophilicity. However, when the textured surface is exposed to the atmosphere, it undergoes wettability transition. The earth's atmosphere consisted of several categories of organic constituents, including long-chain hydrocarbons with carbonyl groups, carboxylic acids, and diol groups. 84 The polar sites on textured AA6061 interacted favorably with the polar groups on volatile organic constituents. It resulted in adsorption of those organic constituents and absorbance of airborne hydrocarbon contamination. 41,44 Adsorption of organic constituents reduced the surface polarity leading to wettability transition to superhydrophobicity.

On the other hand, when the surface was treated with aNLT followed by CIT with different chemical reagents, the wettability of water was stabilized, as shown in Figure 11a. The AA6061 surface treated with aNLT and CIT with the FDDTS reagent remained superhydrophobic over a period of 30 days (Figure 11c). Conversely, the AA6061 surface treated with CPTS after the aNLT process continued to be superhydrophilic, as shown in Figure 11d. Treatment with A-

PFDD and CH₃COONa also resulted in stable superhydrophilicity, as shown in Figure 11e.

CONCLUSIONS

In this study, a systematic methodology is presented to design the surface chemistry of laser-textured metal alloys to alter their extreme wettabilities. All the processed surfaces contain laser-irradiated dual-scale structures with microtrenches covered with micro/nanoscale random features. Laser-textured surface with different combinations of dispersive and non-dispersive components of SFE resulted in three categories of extreme wettabilities.

- I. Surface chemistry that has very low dispersive and nondispersive components of SFE leads to superoleophobicity and superhydrophobicity. This surface energy condition is achieved by attaching -CH₂-, -CF₂-, and -CF₃ groups on top of surface structures.
- II. Surface chemistry with a very high nondispersive component and a high dispersive component of SFE leads to superhydrophilicity and superoleophilicity. The water-affinitive nitrile group (—C=N) is attached to the laser-textured surface to achieve the energy condition. Water molecules tend to create temporary hydrogen bonds with the nitrile group and spread into the microchannel due to the capillary effect leading to superhydrophilicity. On the other hand, diiodomethane spreads on the surface due to the strong capillary effect and relatively higher dispersive SFE.
- III. Surface chemistry that has a very high nondispersive component and a very low dispersive component of SFE leads to the coexistence of superoleophobicity and superhydrophilicity. This surface energy condition is achieved by combining both low-energy $-\mathrm{CF}_2-$ and $-\mathrm{CF}_3$ groups and water-affinitive sodium carboxylate $(-\mathrm{COONa})$ in the same surface chemistry.

The insights from this study will provide design guidance to engineer future surfaces with extreme wettability for emerging applications.

ASSOCIATED CONTENT

Supporting Information

The Supporting Information is available free of charge at https://pubs.acs.org/doi/10.1021/acsami.9b21438.

Experimental conditions of the aNLT step; preparations of the chemical solution of the CIT step; and etching effect during the CIT process and nanostructure enhancement (PDF)

Rolling-off of water and diiodomethane on superoleophobic and superhydrophobic AA6061 surface (MP4)

Water spreading on superhydrophilic AA6061 surface (MP4)

Rolling-off of diiodomethane and spreading of water on AA6061 surface with coexistence of superolephobicity and superhydrophilicity (MP4)

AUTHOR INFORMATION

Corresponding Author

Hongtao Ding — Department of Mechanical Engineering, University of Iowa, Iowa City, Iowa 52242, United States; © orcid.org/0000-0002-0547-1579; Phone: +1-319-335-5674; Email: hongtao-ding@uiowa.edu

Authors

Avik Samanta — Department of Mechanical Engineering,
University of Iowa, Iowa City, Iowa 52242, United States

Wuji Huang — Department of Mechanical Engineering,
University of Iowa, Iowa City, Iowa 52242, United States

Hassan Chaudhry — Department of Mechanical Engineering,
University of Iowa, Iowa City, Iowa 52242, United States

Qinghua Wang — Department of Mechanical Engineering,
University of Iowa, Iowa City, Iowa 52242, United States

Scott K. Shaw — Department of Chemistry, University of Iowa,
Iowa City, Iowa 52242, United States; orcid.org/0000-0003-3767-3236

Complete contact information is available at: https://pubs.acs.org/10.1021/acsami.9b21438

Author Contributions

A.S. conducted the nHSN experiments and surface characterization tests, including contact angle measurement, roll-off angle measurement, SEM analysis, and liquid spreading measurement. W.H. performed the XPS analysis. H.C. and Q.W. helped with the experimental analysis. S.K.S. contributed to the experimental aspects of the investigation. H.D. developed the theoretical concepts, experimental approach, and supervised the investigation. A.S. composed the manuscript. H.D. revised and finalized the manuscript. All participants discussed the results and commented on the manuscript.

Funding

The authors gratefully acknowledge the financial support of the National Science Foundation under grant no. CMMI-1762353.

Notes

The authors declare no competing financial interest.

ACKNOWLEDGMENTS

The authors want to acknowledge Dr. Jun Qu and Dr. Kyungjun Lee from Materials Science and Technology Division at Oak Ridge National Laboratory for useful discussion on the surface free energy and Prof. Hui Hu from Iowa State University for his assistance with high-speed images of water droplet spreading. The authors also would like to thank Majid H. Nada and Prof. Sarah C. Larsen from the Department of Chemistry at the University of Iowa for their help with the ICP-OES experiments and Phil Pagano and Kenny Horkley from University of Iowa MATFAB facility for XPS measurements.

REFERENCES

- (1) Chen, F.; Zhang, D.; Yang, Q.; Yong, J.; Du, G.; Si, J.; Yun, F.; Hou, X. Bioinspired Wetting Surface via Laser Microfabrication. ACS Appl. Mater. Interfaces 2013, 5, 6777–6792.
- (2) Yoon, Y.; Kim, D.; Lee, J.-B. Hierarchical Micro/Nano Structures for Super-Hydrophobic Surfaces and Super-Lyophobic Surface against Liquid Metal. *Micro Nano Syst. Lett.* **2014**, *2*, 3.
- (3) Zeira, A.; Chowdhury, D.; Hoeppener, S.; Liu, S.; Berson, J.; Cohen, S. R.; Maoz, R.; Sagiv, J. Patterned Organosilane Monolayers as Lyophobic-Lyophilic Guiding Templates in Surface Self-Assembly: Monolayer Self-Assembly versus Wetting-Driven Self-Assembly. *Langmuir* 2009, 25, 13984–14001.
- (4) Chu, Z.; Seeger, S. Superamphiphobic Surfaces. Chem. Soc. Rev. 2014, 43, 2784–2798.

- (5) Meng, C.; Wang, B.; Gao, Z.; Liu, Z.; Zhang, Q.; Zhai, J. Insight into the Role of Surface Wettability in Electrocatalytic Hydrogen Evolution Reactions Using Light-Sensitive Nanotubular TiO₂ Supported Pt Electrodes. *Sci. Rep.* **2017**, *7*, 41825.
- (6) Habedank, J. B.; Günter, F. J.; Billot, N.; Gilles, R.; Neuwirth, T.; Reinhart, G.; Zaeh, M. F. Rapid Electrolyte Wetting of Lithium-Ion Batteries Containing Laser Structured Electrodes: In Situ Visualization by Neutron Radiography. *Int. J. Adv. Manuf. Technol.* **2019**, 2769
- (7) Pfleging, W.; Pröll, J. A New Approach for Rapid Electrolyte Wetting in Tape Cast Electrodes for Lithium-Ion Batteries. *J. Mater. Chem. A* **2014**, *2*, 14918–14926.
- (8) Takata, Y.; Hidaka, S.; Cao, J. M.; Nakamura, T.; Yamamoto, H.; Masuda, M.; Ito, T. Effect of Surface Wettability on Boiling and Evaporation. *Energy* **2005**, *30*, 209–220.
- (9) Ferraris, S.; Bobbio, A.; Miola, M.; Spriano, S. Micro- and Nano-Textured, Hydrophilic and Bioactive Titanium Dental Implants. *Surf. Coat. Technol.* **2015**, *276*, 374–383.
- (10) Ferrari, M.; Benedetti, A.; Santini, E.; Ravera, F.; Liggieri, L.; Guzman, E.; Cirisano, F. Biofouling Control by Superhydrophobic Surfaces in Shallow Euphotic Seawater. *Colloids Surf., A* **2015**, *480*, 369–375.
- (11) Ellinas, K.; Kefallinou, D.; Stamatakis, K.; Gogolides, E.; Tserepi, A. Is There a Threshold in the Antibacterial Action of Superhydrophobic Surfaces? *ACS Appl. Mater. Interfaces* **2017**, *9*, 39781–39789.
- (12) Samaha, M. A.; Tafreshi, H. V.; Gad-el-Hak, M. Superhydrophobic Surfaces: From the Lotus Leaf to the Submarine. *C. R. Mec.* **2012**, *340*, 18–34.
- (13) Gose, J. W.; Golovin, K.; Boban, M.; Mabry, J. M.; Tuteja, A.; Perlin, M.; Ceccio, S. L. Characterization of Superhydrophobic Surfaces for Drag Reduction in Turbulent Flow. *J. Fluid Mech.* **2018**, 845, 560–580.
- (14) Wei, D.; Wang, J.; Wang, H.; Liu, Y.; Li, S.; Li, D. Anti-Corrosion Behaviour of Superwetting Structured Surfaces on Mg-9Al-1Zn Magnesium Alloy. *Appl. Surf. Sci.* **2019**, *483*, 1017–1026.
- (15) Tudu, B. K.; Kumar, A.; Bhushan, B. Facile Approach to Develop Anti-Corrosive Superhydrophobic Aluminium with High Mechanical, Chemical and Thermal Durability. *Philos. Trans. R. Soc., A* **2019**, 377, 20180272.
- (16) Bhushan, B.; Jung, Y. C.; Koch, K. Self-Cleaning Efficiency of Artificial Superhydrophobic Surfaces. *Langmuir* **2009**, 25, 3240–3248.
- (17) Lee, K.; Lyu, S.; Lee, S.; Kim, Y. S.; Hwang, W. Characteristics and Self-Cleaning Effect of the Transparent Super-Hydrophobic Film Having Nanofibers Array Structures. *Appl. Surf. Sci.* **2010**, 256, 6729–6735.
- (18) Liu, Y.; Li, L.; Li, H.; Hu, H. An Experimental Study of Surface Wettability Effects on Dynamic Ice Accretion Process over an UAS Propeller Model. *Aerosp. Sci. Technol.* **2018**, *73*, 164–172.
- (19) Farhadi, S.; Farzaneh, M.; Kulinich, S. A. Anti-Icing Performance of Superhydrophobic Surfaces. *Appl. Surf. Sci.* **2011**, 257, 6264–6269.
- (20) Yang, J.; Zhang, Z.; Xu, X.; Zhu, X.; Men, X.; Zhou, X. Superhydrophilic-Superoleophobic Coatings. *J. Mater. Chem.* **2012**, 22, 2834–2837.
- (21) Eick, J. D.; Johnson, L. N.; Fromer, J. R.; Good, R. J.; Neumann, A. W. Surface Topography: Its Influence on Wetting and Adhesion in a Dental Adhesive System. *J. Dent. Res.* **1972**, *51*, 780–788
- (22) Jeevahan, J.; Chandrasekaran, M.; Britto Joseph, G.; Durairaj, R. B.; Mageshwaran, G. Superhydrophobic Surfaces: A Review on Fundamentals, Applications, and Challenges. *J. Coat. Technol. Res.* **2018**, *15*, 231–250.
- (23) Otitoju, T. A.; Ahmad, A. L.; Ooi, B. S. Superhydrophilic (Superwetting) Surfaces: A Review on Fabrication and Application. *J. Ind. Eng. Chem.* **2017**, *47*, 19–40.
- (24) Vorobyev, A. Y.; Guo, C. Multifunctional Surfaces Produced by Femtosecond Laser Pulses. J. Appl. Phys. 2015, 117, 033103.

- (25) Vorobyev, A. Y.; Guo, C. Femtosecond Laser Structuring of Titanium Implants. *Appl. Surf. Sci.* **2007**, 253, 7272–7280.
- (26) Vorobyev, A. Y.; Makin, V. S.; Guo, C. Periodic Ordering of Random Surface Nanostructures Induced by Femtosecond Laser Pulses on Metals. *J. Appl. Phys.* **2007**, *101*, 034903.
- (27) Martínez-Calderon, M.; Rodríguez, A.; Dias-Ponte, A.; Morant-Miñana, M. C.; Gómez-Aranzadi, M.; Olaizola, S. M. Femtosecond Laser Fabrication of Highly Hydrophobic Stainless Steel Surface with Hierarchical Structures Fabricated by Combining Ordered Microstructures and LIPSS. *Appl. Surf. Sci.* **2016**, *374*, 81–89.
- (28) Rukosuyev, M. V.; Lee, J.; Cho, S. J.; Lim, G.; Jun, M. B. G. One-Step Fabrication of Superhydrophobic Hierarchical Structures by Femtosecond Laser Ablation. *Appl. Surf. Sci.* **2014**, *313*, 411–417.
- (29) Tanvir Ahmmed, K. M.; Grambow, C.; Kietzig, A.-M. Fabrication of Micro/Nano Structures on Metals by Femtosecond Laser Micromachining. *Micromachines* **2014**, *5*, 1219–1253.
- (30) Li, B. j.; Li, H.; Huang, L. j.; Ren, N. f.; Kong, X. Femtosecond Pulsed Laser Textured Titanium Surfaces with Stable Superhydrophilicity and Superhydrophobicity. *Appl. Surf. Sci.* **2016**, 389, 585–593.
- (31) Zhang, D.; Sugioka, K. Hierarchical Microstructures with High Spatial Frequency Laser Induced Periodic Surface Structures Possessing Different Orientations Created by Femtosecond Laser Ablation of Silicon in Liquids. *Opto-Electronic Adv.* **2019**, *2*, 190002.
- (32) Zhang, Z.; Gu, Q.; Jiang, W.; Zhu, H.; Xu, K.; Ren, Y.; Xu, C. Achieving of Bionic Super-Hydrophobicity by Electrodepositing Nano-Ni-Pyramids on the Picosecond Laser-Ablated Micro-Cu-Cone Surface. Surf. Coat. Technol. 2019, 363, 170–178.
- (33) Jagdheesh, R.; Diaz, M.; Ocaña, J. L. Bio Inspired Self-Cleaning Ultrahydrophobic Aluminium Surface by Laser Processing. *RSC Adv.* **2016**, *6*, 72933–72941.
- (34) Chun, D. M.; Ngo, C. V.; Lee, K. M. Fast Fabrication of Superhydrophobic Metallic Surface Using Nanosecond Laser Texturing and Low-Temperature Annealing. *CIRP Ann.* **2016**, *65*, 519–522.
- (35) Ta, V. D.; Dunn, A.; Wasley, T. J.; Li, J.; Kay, R. W.; Stringer, J.; Smith, P. J.; Esenturk, E.; Connaughton, C.; Shephard, J. D. Laser Textured Surface Gradients. *Appl. Surf. Sci.* **2016**, *371*, 583–589.
- (36) Jagdheesh, R.; García-Ballesteros, J. J.; Ocaña, J. L. One-Step Fabrication of near Superhydrophobic Aluminum Surface by Nanosecond Laser Ablation. *Appl. Surf. Sci.* **2016**, *374*, 2–11.
- (37) Ukar, E.; Lamikiz, A.; Martínez, S.; Arrizubieta, I. Laser Texturing with Conventional Fiber Laser. *Procedia Eng.* **2015**, *132*, 663–670.
- (38) Farrokhi, H.; Zhou, W.; Zheng, H. Y. Silicon Surface Texturing by Forming Sub-Micron Bumps with a CW Fiber Laser. In *Proceedings of the 13th International Conference of the European Society for Precision Engineering and Nanotechnology, EUSPEN 2013*; Euspen: Cranfield, U.K., 2013; 2, pp 273–276.
- (39) Farrokhi, H.; Zhou, W.; Zheng, H. Y.; Li, Z. L. Non-Ablative Texturing of Silicon Surface with a Continuous Wave Fiber Laser. Opt. Express 2012, 20, 23180.
- (40) Pendurthi, A.; Movafaghi, S.; Wang, W.; Shadman, S.; Yalin, A. P.; Kota, A. K. Fabrication of Nanostructured Omniphobic and Superomniphobic Surfaces with Inexpensive CO2Laser Engraver. ACS Appl. Mater. Interfaces 2017, 9, 25656–25661.
- (41) Long, J.; Zhong, M.; Zhang, H.; Fan, P. Superhydrophilicity to Superhydrophobicity Transition of Picosecond Laser Microstructured Aluminum in Ambient Air. J. Colloid Interface Sci. 2015, 441, 1–9.
- (42) Wu, B.; Zhou, M.; Li, J.; Ye, X.; Li, G.; Cai, L. Superhydrophobic Surfaces Fabricated by Microstructuring of Stainless Steel Using a Femtosecond Laser. *Appl. Surf. Sci.* **2009**, 256, 61–66.
- (43) Boinovich, L. B.; Emelyanenko, A. M.; Emelyanenko, K. A.; Domantovsky, A. G.; Shiryaev, A. A. Comment on "Nanosecond Laser Textured Superhydrophobic Metallic Surfaces and Their Chemical Sensing Applications" by Duong V. Ta, Andrew Dunn, Thomas J. Wasley, Robert W. Kay, Jonathan Stringer, Patrick J. Smith,

- Colm Connaughton, Jonathan D. Shephard (Appl. Surf. Sci. 357 (2015) 248–254). Appl. Surf. Sci. 2016, 379, 111–113.
- (44) Bizi-Bandoki, P.; Valette, S.; Audouard, E.; Benayoun, S. Time Dependency of the Hydrophilicity and Hydrophobicity of Metallic Alloys Subjected to Femtosecond Laser Irradiations. *Appl. Surf. Sci.* **2013**, 273, 399–407.
- (45) Ngo, C.-V.; Chun, D.-M. Effect of Heat Treatment Temperature on the Wettability Transition from Hydrophilic to Superhydrophobic on Laser-Ablated Metallic Surfaces. *Adv. Eng. Mater.* **2018**, *20*, 1701086.
- (46) Tang, M. K.; Huang, X. J.; Guo, Z.; Yu, J. G.; Li, X. W.; Zhang, Q. X. Fabrication of Robust and Stable Superhydrophobic Surface by a Convenient, Low-Cost and Efficient Laser Marking Approach. *Colloids Surf.*, A 2015, 484, 449–456.
- (47) Yan, H.; Abdul Rashid, M. R. B.; Khew, S. Y.; Li, F.; Hong, M. Wettability Transition of Laser Textured Brass Surfaces inside Different Mediums. *Appl. Surf. Sci.* **2018**, *427*, 369–375.
- (48) Wang, Q.; Samanta, A.; Shaw, S. K.; Hu, H.; Ding, H. Nanosecond Laser-Based High-Throughput Surface Nanostructuring (NHSN). *Appl. Surf. Sci.* **2020**, *507*, 145136.
- (49) Samanta, A.; Wang, Q.; Singh, G.; Shaw, S. K.; Toor, F.; Ratner, A.; Ding, H. Nanosecond Pulsed Laser Processing Turns Engineering Metal Alloys Antireflective and Superwicking. *J. Manuf. Process.* **2020**, *54*, 28–37.
- (50) Ngo, C. V.; Chun, D. M. Control of Laser-Ablated Aluminum Surface Wettability to Superhydrophobic or Superhydrophilic through Simple Heat Treatment or Water Boiling Post-Processing. *Appl. Surf. Sci.* **2018**, *435*, 974–982.
- (51) Liu, D.; Yu, Y.; Chen, X.; Zheng, Y. Selective Separation of Oil and Water with Special Wettability Mesh Membranes. *RSC Adv.* **2017**, *7*, 12908–12915.
- (52) Pan, Y.; Huang, S.; Li, F.; Zhao, X.; Wang, W. Coexistence of Superhydrophilicity and Superoleophobicity: Theory, Experiments and Applications in Oil/Water Separation. *J. Mater. Chem. A* **2018**, *6*, 15057–15063.
- (53) Yang, J.; Song, H.; Yan, X.; Tang, H.; Li, C. Superhydrophilic and Superoleophobic Chitosan-Based Nanocomposite Coatings for Oil/Water Separation. *Cellulose* **2014**, *21*, 1851–1857.
- (54) Qu, M.; Ma, L.; Zhou, Y.; Zhao, Y.; Wang, J.; Zhang, Y.; Zhu, X.; Liu, X.; He, J. Durable and Recyclable Superhydrophilic—Superoleophobic Materials for Efficient Oil/Water Separation and Water-Soluble Dyes Removal. ACS Appl. Nano Mater. 2018, 1, 5197—5209.
- (55) Wang, B.; Liang, W.; Guo, Z.; Liu, W. Biomimetic Super-Lyophobic and Super-Lyophilic Materials Applied for Oil/Water Separation: A New Strategy beyond Nature. *Chem. Soc. Rev.* **2015**, *44*, 336–361.
- (56) Wang, Y.; Gong, X. Special Oleophobic and Hydrophilic Surfaces: Approaches, Mechanisms, and Applications. *J. Mater. Chem. A* **2017**, *5*, 3759–3773.
- (57) Girifalco, L. A.; Good, R. J. A Theory for the Estimation of Surface and Interfacial Energies. I. Derivation and Application to Interfacial Tension. *J. Phys. Chem.* **1957**, *61*, 904–909.
- (58) Fowkes, F. M. Attractive Forces At Interfaces. *Ind. Eng. Chem.* **1964**, 56, 40–52.
- (59) Jarvis, N. L.; Zisman, W. A. Surface Chemistry of Fluorochemicals. In *Kirk-Othmer Encyclopedia of Chemical Technology*; John Wiley & Sons: New York, 1965; pp 707–738.
- (60) Ouellette, R. J.; Rawn, J. D. Structure and Bonding in Organic Compounds. In *Organic Chemistry*; Academic Press: 2018; pp 1–30, DOI: 10.1016/B978-0-12-812838-1.50001-3.
- (61) Robert, J. D.; Caserio, M. C. Carbonyl Compounds I: Aldehydes and Ketones. Addition Reactions of the Carbonyl Group. In *Basic Principles of Organic Chemistry*; WA Benjamin, Inc.: 1977.
- (62) Wenzel, R. N. Resistance of Solid Surfaces to Wetting by Water. *Ind. Eng. Chem.* **1936**, 28, 988–994.
- (63) Cassie, A. B. D.; Baxter, S. Wettability of Porous Surfaces. *Trans. Faraday Soc.* **1944**, *40*, 546–551.

- (64) Ding, H.; Wang, Q.; Samanta, A.; Shen, N. Nanosecond Laser-Based High-Throughput Surface Nano-Structuring (NHSN) Process. US 20,190,054,571 A1, 2019.
- (65) Liu, Y.; Zhang, Z.; Hu, H.; Hu, H.; Samanta, A.; Wang, Q.; Ding, H. An Experimental Study to Characterize a Surface Treated with a Novel Laser Surface Texturing Technique: Water Repellency and Reduced Ice Adhesion. Surf. Coat. Technol. 2019, 374, 634–644.
- (66) Samanta, A.; Wang, Q.; Shaw, S. K.; Ding, H. Nanostructuring of Laser Textured Surface to Achieve Superhydrophobicity on Engineering Metal Surface. *J. Laser Appl.* **2019**, *31*, No. 022515.
- (67) Samanta, A.; Singh, G.; Wang, Q.; Shaw, S. K.; Ratner, A.; Hu, H.; Ding, H. Enable Superwicking in Metal Alloys via a Laser-Chemical Surface Treatment Method. J. Mater. Process. Technol. 2020 Under Revi.
- (68) Chang, F.-M.; Cheng, S.-L.; Hong, S.-J.; Sheng, Y.-J.; Tsao, H. K. Superhydrophilicity to Superhydrophobicity Transition of CuO Nanowire Films. *Appl. Phys. Lett.* **2010**, *96*, 114101.
- (69) Chen, T.; Liu, H.; Yang, H.; Yan, W.; Zhu, W.; Liu, H. Biomimetic Fabrication of Robust Self-Assembly Superhydrophobic Surfaces with Corrosion Resistance Properties on Stainless Steel Substrate. *RSC Adv.* **2016**, *6*, 43937–43949.
- (70) Mousa, A.; Heinrich, G.; Simon, F.; Wagenknecht, U.; Stöckelhuber, K.-W.; Dweiri, R. Carboxylated Nitrile Butadiene Rubber/Hybrid Filler Composites. *Mater. Res.* **2012**, *15*, 671–678.
- (71) Younesi, R.; Norby, P.; Vegge, T. A New Look at the Stability of Dimethyl Sulfoxide and Acetonitrile in Li-O2 Batteries. *ECS Electrochem. Lett.* **2014**, 3, A15–A18.
- (72) Ferraria, A. M.; Lopes da Silva, J. D.; Botelho do Rego, A. M. XPS Studies of Directly Fluorinated HDPE: Problems and Solutions. *Polymer* **2003**, *44*, 7241–7249.
- (73) Meng, L.; Zhang, X.; Tang, Y.; Su, K.; Kong, J. Hierarchically Porous Silicon-Carbon-Nitrogen Hybrid Materials towards Highly Efficient and Selective Adsorption of Organic Dyes. *Sci. Rep.* **2015**, *5*, 1
- (74) Wang, Y. Y.; Kusumoto, K.; Li, C. J. XPS Analysis of SiC Films Prepared by Radio Frequency Plasma Sputtering. *Phys. Procedia* **2012**, 32, 95–102.
- (75) Raphaël, E. Capillary Rise of a Wetting Fluid in a Semi-Circular Groove. *J. Phys.* **1989**, *50*, 485–491.
- (76) Gregorčič, P.; Šetina-Batič, B.; Hočevar, M. Controlling the Stainless Steel Surface Wettability by Nanosecond Direct Laser Texturing at High Fluences. *Appl. Phys. A: Mater. Sci. Process.* **2017**, 123, 766.
- (77) Kietzig, A. M.; Hatzikiriakos, S. G.; Englezos, P. Patterned Superhydrophobic Metallic Surfaces. *Langmuir* **2009**, 25, 4821–4827. (78) Ta, D. V.; Dunn, A.; Wasley, T. J.; Kay, R. W.; Stringer, J.; Smith, P. J.; Connaughton, C.; Shephard, J. D. Nanosecond Laser Textured Superhydrophobic Metallic Surfaces and Their Chemical Sensing Applications. *Appl. Surf. Sci.* **2015**, 357, 248–254.
- (79) Tang, M.; Shim, V.; Pan, Z. Y.; Choo, Y. S.; Hong, M. H. Laser Ablation of Metal Substrates for Super-Hydrophobic Effect. *J. Laser Micro/Nanoeng.* **2011**, *6*, 6–9.
- (80) Yang, Ž.; Tian, Y. L.; Yang, C. J.; Wang, F. J.; Liu, X. P. Modification of Wetting Property of Inconel 718 Surface by Nanosecond Laser Texturing. *Appl. Surf. Sci.* **2017**, *414*, 313–324.
- (81) Tian, Y.; Jiang, L. Wetting: Intrinsically Robust Hydrophobicity. *Nat. Mater.* **2013**, 12, 291–292.
- (82) Gentleman, M. M.; Ruud, J. A. Role of Hydroxyls in Oxide Wettability. *Langmuir* **2010**, *26*, 1408–1411.
- (83) Azimi, G.; Dhiman, R.; Kwon, H. M.; Paxson, A. T.; Varanasi, K. K. Hydrophobicity of Rare-Earth Oxide Ceramics. *Nat. Mater.* **2013**, *12*, 315–320.
- (84) Goldstein, A. H.; Galbally, I. E. Known and Unexplored Organic Constituents in the Earth's Atmosphere. *Environ. Sci. Technol.* **2007**, *41*, 1514–1521.